JACS
JOURNAL OF THE AMERICAN CHEMICAL SOCIETY
pubs.acs.org/JACS
Communication

Synthesis of Sb_{68}^{8-}: Crafting a Homoatomic Antimony Nanotorus

Yun Zhang, Wen-Juan Tian, Wei-Xing Chen, Manfred Scheer, and Zhong-Ming Sun*

Cite This: J. Am. Chem. Soc. 2024, 146, 27977−27982
Read Online
ACCESS | Metrics & More | Article Recommendations | Supporting Information

ABSTRACT: Pure-element cyclic molecules have garnered extensive attention owing to their intriguing structures and promising applications. Among these, carbon-based cyclic molecules such as *cyclo*[*n*]carbon (C_n, n = 10−26) and carbon nanotori have ignited significant interest in both experimental and theoretical investigations. However, systematic investigations of analogous cyclic counterparts of heavier main-group elements are limited, with only a few known by theoretical studies. Furthermore, these corresponding cyclic structures lack synthetic examples in the condensed phase, primarily attributed to their high reactivity resulting from lone electron pairs and the absence of electronic delocalization, which typically aids in stabilizing the structure. In this work, we introduce the pioneering synthesis of a pure antimony-based inorganic nanotorus, denoted as Sb_{68}^{8-}, facilitated by the incorporation of C_{60} for oxidation by utilizing wet-chemistry methodologies. The unique nanotorus structure was meticulously examined via single-crystalline X-ray diffraction, unveiling its composition of 68 antimony atoms and forming a tubular structure with approximate dimensions of 18.5 × 18.4 Å^2 in a square shape. Theoretical calculations further revealed that the nanotorus structure, characterized by 16 delocalized electrons distributed across eight 3c-2e σ bonds, effectively saturated the eight two-coordinated Sb atoms within the cluster. This study unveils an innovative approach to synthesizing cyclic compounds solely from pure elements, departing from traditional methods dependent on chemical vapor deposition or surface synthesis, and heralds a profound paradigm shift in physical science.

Downloaded via NANKAI UNIV on October 24, 2024 at 00:47:21 (UTC).
See https://pubs.acs.org/sharingguidelines for options on how to legitimately share published articles.

Deliberately designed cyclic compounds, particularly those composed of pure elements, have emerged as a key focus in synthetic chemistry,[1,2] attracting widespread interest. Previous studies have underscored the significance of cyclic carbon-based molecules[3] and nanotori materials.[4,5] Surface synthesis techniques have been employed to generate *cyclo*[*n*]-carbons (C_n, n = 10, 13, 14, 16, 18, and 26),[6−9] and the electronic structures of these molecules were elucidated through atomic force microscopy and theoretical calculations. These studies confirmed the aromaticity of C_{10}, C_{14}, and C_{18},[6,7] while C_{16}[8] exhibits a double antiaromaticity (Figure 1a). Additionally, ring-like fullerenes, commonly known as carbon nanotori (Figure 1b), represent a significant category of single-wall carbon nanotubes (SWNTs).[10,11] These investigations into the theoretical predictions, synthesis, and applications of carbon nanotori with various nuclearities have consistently captured significant interest.[12,13] In particular, there has been a focus on exploring the feasibility of carbon nanotori for encapsulating chains of metallic atoms[11] and their potential use as nanoscale oscillators in nanoelectromechanical systems.[14]

In contrast to carbon, molecular compounds composed of heavier group 15 elements, such as P, As, and Sb, exhibit limited stability due to the increased reactivity of their lone electron pairs.[15] This high reactivity has posed a significant challenge to the synthesis of corresponding cyclic compounds, which has remained largely elusive. Interestingly, theoretical investigations have highlighted the energetic stability of such inorganic cyclic compounds. For instance, a series of cyclic compounds of Pn_m (Pn = P, As; m = 80−360), which are composed of recurring realgar-type Pn_8 and Pn_2 moieties (Figure 1c), have been theoretically predicted.[16−18] Recently,

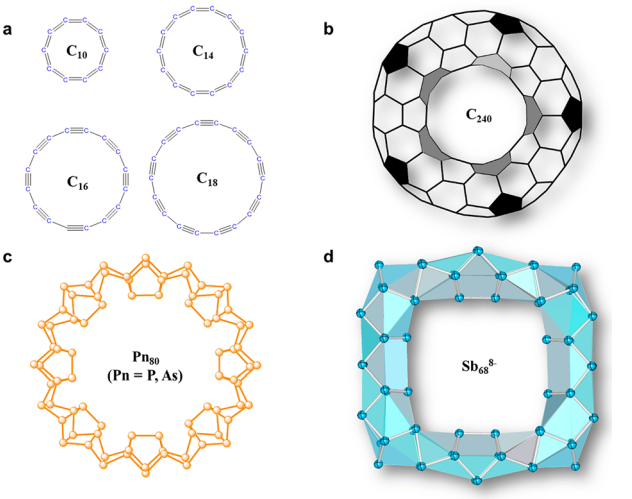

Figure 1. Selected instances of the pure element cyclic molecules. (a) *Cyclo*[*n*]carbon, n = 10−26. (b) A toroidal isomer of the carbon nanotori. (c) Predicted *cyclo*-phosphene and *cyclo*-arsenene in theoretical chemistry (Pn_{80}, Pn = P, As). (d) This work.

Received: July 5, 2024
Revised: September 18, 2024
Accepted: September 21, 2024
Published: September 27, 2024

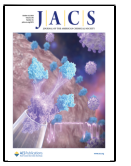

© 2024 American Chemical Society

https://doi.org/10.1021/jacs.4c09102
J. Am. Chem. Soc. 2024, 146, 27977−27982

Scheme 1. Synthesis Route of $[K(18\text{-crown-}6)\cdot DMF]_8[Sb_{68}]\cdot tol$

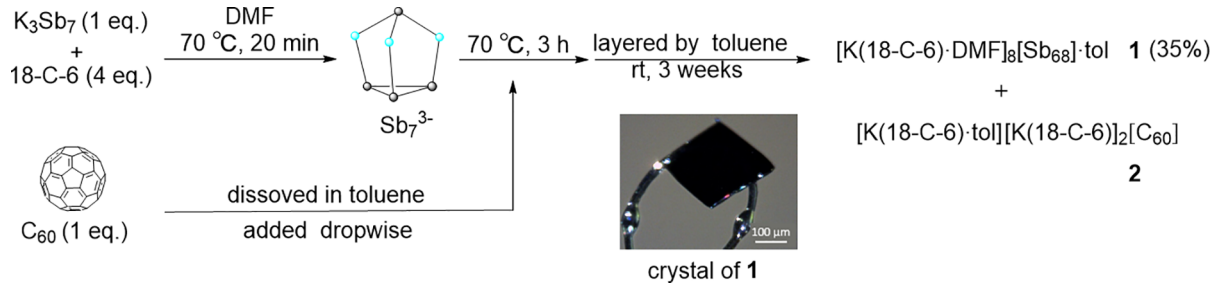

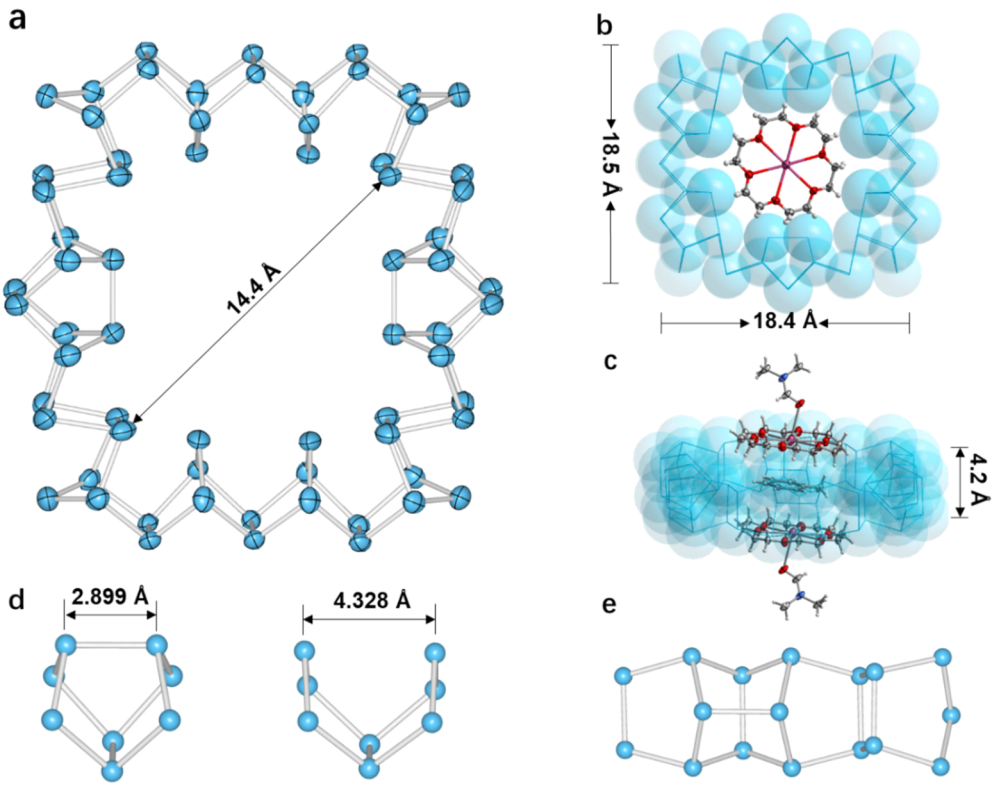

Figure 2. Anionic structure of Sb_{68}^{8-} with 50% probability thermal ellipsoids (a). The interaction between the 18-c-6 molecule and the Sb_{68} anion from different angles: top view (b) and side view (c). (d) Contains two Sb_8 units. (e) A typical Sb_{17} subunit.

employing chemical vapor deposition (CVT) within carbon nanotube reactors has emerged as a practical method for synthesizing linear or ring-shaped phosphene and arsenene entities.[19−22] Cyclic phosphene was synthesized within carbon nanotube nanoreactors using CVT and reaction assembly techniques.[15] However, employing multiwalled carbon nanotubes as protective carriers for the embedding of such ring systems has become essential, presenting ongoing challenges for their precise structural characterization. As a result, there are still no concrete examples known for the synthesis of pure-element inorganic cyclic compounds in the condensed phase. The s^2p^3 electron configuration of P, As, and Sb atoms achieves stability when it attains an eight-electron closed-shell configuration, promoting the formation of grid-like covalent structures in the condensed phase,[23] thereby hindering the synthesis of cyclic compounds. In prior research, various chain-like structures, including P_{16}^{2-},[24] P_{21}^{3-},[25] P_{26}^{4-},[26,27] and As_{21}^{3-},[28] were synthesized using techniques such as the cleavage coupling of white phosphorus and oxidation-facilitated fusion of Zintl ions. By delving into synthetic strategies for these clusters, it is envisaged that employing appropriate oxidants for further oxidation of these chain-like clusters could facilitate the formation of cyclic structures or even larger chain-like structures.[29] These findings suggest that antimony may also have the potential to form analogous structures. However, until now, there have been no documented successful examples of related polyantimony clusters experimentally. This may be attributed to the robust metallic feature of Sb and the lack of identified mild and compatible oxidants.

In this study, we present the inaugural synthesis of the first pure antimony-based inorganic nanotorus, Sb_{68}^{8-} (Figure 1d). The unique nanotorus structure was meticulously analyzed through single-crystal X-ray diffraction. Our approach employs wet chemistry techniques, leveraging the self-assembly and oxidation coupling behavior of antimony. By utilizing C_{60} as a mild oxidant, the Zintl precursor K_3Sb_7 undergoes oxidative coupling, which potentially generates linear building blocks, culminating in a self-assembly of a pure antimony nanotorus. This method represents the first-ever synthesis of a maximal

https://doi.org/10.1021/jacs.4c09102
J. Am. Chem. Soc. 2024, 146, 27977−27982

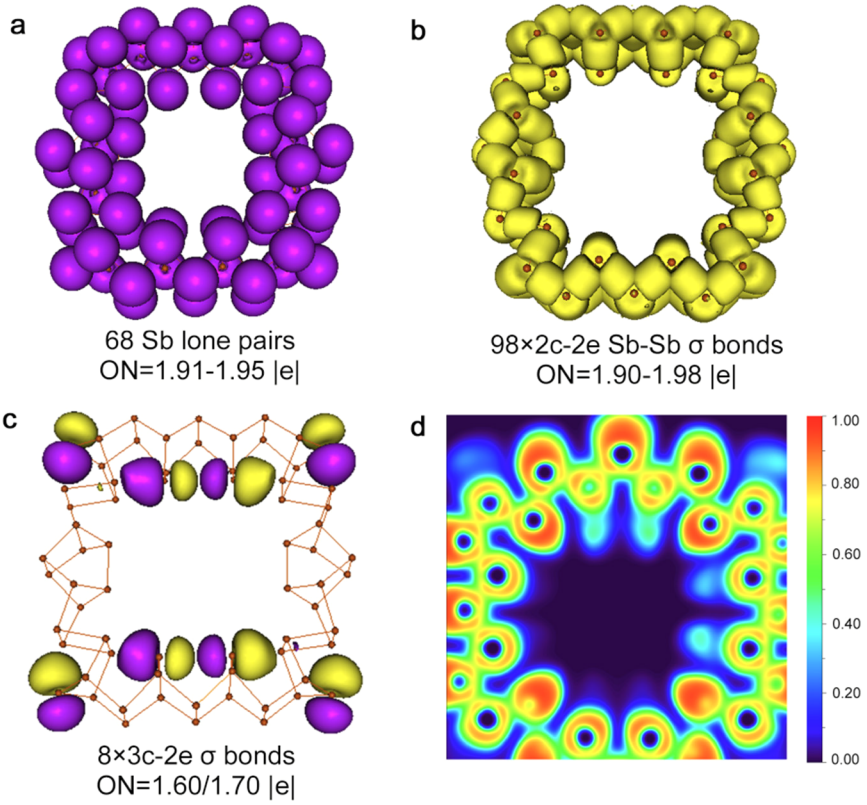

Figure 3. Chemical bonding pattern of Sb_{68}^{8-} obtained from AdNDP and ELF analysis. (a, b) Lewis bonding elements, including lone pairs and 2c-2e bonds. (c) Eight Sb−Sb−Sb 3c-2e σ bonds. Occupation numbers (ONs) are shown. (d) ELF plot of Sb_{68}^{8-} in the plane taken through the surface of the cluster and parallel to the radial plane of the cluster.

all-metal molecular torus, also providing initial evidence that C_{60} exhibits mild oxidizing properties in main group metal cluster chemistry.

SYNTHESIS AND STRUCTURAL ANALYSIS

Given the mild oxidative properties[30] of C_{60} and the notable assembly and coordination capabilities of antimony atoms within Zintl cluster chemistry, we utilized a coordination-driven self-assembly strategy[31] to combine antimony-based Zintl ions with C_{60}, successfully synthesizing compound **1** $[K(18\text{-c-}6)\cdot DMF]_8[Sb_{68}]\cdot tol$ (18-c-6 = 1,4,7,10,13,16-hexaoxacyclo-octadecane, tol = toluene) (vide infra). The reaction of the Zintl precursor K_3Sb_7 in DMF (dimethylformamide) with C_{60} in the presence of 18-crown-6 was conducted by maintaining the reaction system at 70 °C for 3 hours. After a storage period of 3 weeks, black plate-like crystals of compound **1** were obtained with a 35% crystalline yield (Scheme1). Interestingly, a small amount of black block-like crystals of compound **2** was observed in the reaction solution after one month. Single-crystalline X-ray diffraction analysis revealed that compound **2** is identical to the previously reported trianionic species C_{60}^{3-},[32] coordinated by three $[K(18\text{-c-}6)]^+$ cations, providing direct evidence that C_{60} acts as an oxidizing agent during the synthesis of Sb_{68}^{8-}. The Sb_{68}^{8-} cluster exhibited a prevailing tendency to decompose upon exposure to ambient air, which was attributed to its large nuclearity and high negative charge. Electrospray ionization mass spectrometry (ESI-MS) of freshly prepared DMF solutions of **1** identified only a few relevant fragment peaks at m/z = 2069.3344, 2313.1953, and 2800.7885, corresponding to $[Sb_{17}]^-$, $[Sb_{19}]^-$, and $[Sb_{23}]^-$ ions (Figures S6−8). This suggests that under gas-phase testing conditions, the parent cluster $[Sb_{68}]^{8-}$ is highly unstable and prone to fragmentation into smaller pieces. This finding also implies that relevant fragment species may play a crucial role in the construction or assembly of the parent cluster. Energy dispersive X-ray (EDX) analysis results indicate that the atomic ratio of K to Sb is 8.3:68, which aligns closely with the calculated value (Figure S9).

Crystallographic analysis revealed that $[K(18\text{-c-}6)\cdot DMF]_8[Sb_{68}]\cdot tol$ crystallizes in the triclinic space group $P\bar{1}$, and the unit cell contains one Sb_{68}^{8-} anion, eight $[K(18\text{-c-}6)\cdot DMF]^+$ cations surrounding the antimony cluster, and one toluene molecule positioned in the center of the Sb_{68} nanotorus (refer to Figures S2 and 3). Analysis of the cluster structure (Figure 2) revealed a "torus-like" anion with 68 antimony atoms, which is composed of four edges. Each of the four edges comprises an Sb_8 unit: one exhibits a realgar-type configuration, which is isostructural with the Sb_8 unit present in the $[(LMg)_4Sb_8]$ complex,[33] characterized by an Sb−Sb bond length of 2.899 Å. The other features a pocket-like Sb_8 structure, with an Sb···Sb distance of 4.328 Å (Figure 2d). It is hypothesized that the formation of the pocket-like Sb_8 structure may result from the cleavage of Sb−Sb bonds within the realgar-type configuration during the fusion process. Additionally, the external dimensions of the cluster are approximately 18.5 Å in length, 18.4 Å in width, and 4.2 Å in height, with an internal cavity measuring about 14.4 Å. This suggests that the spatial characteristics of the cluster are similar to those of carbon nanotori in host−guest recognition domains.[11] The $[K(18\text{-c-}6)]\cdot tol\cdot[K(18\text{-c-}6)]$ moiety lies at the center of the nanotorus cluster, forming a "sandwich-like"

https://doi.org/10.1021/jacs.4c09102
J. Am. Chem. Soc. 2024, 146, 27977−27982

structure (Figure 2c). This component significantly influences the self-assembly process, and substituting the cation capture agent with a [2.2.2]crypt molecule results in the absence of any observable crystallized product. The complete encapsulation of K^+ ions by the [2.2.2]crypt impedes their coordination with toluene. The Sb−Sb bond lengths within the Sb_{68}^{8-} cluster anion range from 2.757(1) to 3.077(1) Å, with an average bond length of 2.825 Å. Notably, eight bond lengths within cluster **1**, which range from 2.913(1) to 3.077(1) Å, are comparatively longer than those of typical Sb−Sb single bonds (2.820 Å).[34] The other bond lengths range from 2.757(1) to 2.899(1) Å, closely match single-bond distances,[35] and align with the bond length range within the classical Sb_7^{3-} anion, which spans from 2.717(4) to 2.906(2) Å.[34] According to the 8-*N* rule, the bonding of the eight Sb atoms in the cluster, each in a two-coordinate environment, is not fully saturated. Therefore, each of these Sb atoms formally carries a negative charge. Alternatively, this stability can also be interpreted in terms of the "average reduction state", in which the cluster charge is divided by the overall number of atoms in the cluster.[29]

Moreover, the repeating units (Sb_2/Sb_8) in **1** on two sides of the wheel are similar to sections of Hittorf's phosphorus or the linear phosphorus modification,[20,36] in which P_9 units are responsible for linking the $P_2/P_8/P_2/P_9$ strands together by P−P single bonds. This feature is almost unknown for polyantimony units, due to the very low Sb−Sb single-bond energy. Exceptions of homoatomic polyantimony chains with Sb−Sb single bonds have only been found recently.[37] Compared to these cyclic chains in $[(NbCp)_2Sb_{10}]^{2-}$, $[MSb_{13}]^{3-}$ (M = Ru/Fe), and $[MSb_{15}]^{3-}$ (M = Ru/Fe), the Sb_{68}^{8-} cluster does not require transition metals for stabilization and forms a nonclassical cyclic structure (i.e., a non-monatomic ring). However, this leak of Sb−Sb single-bond formation might be the reason that nanowheel Sb_{68}^{8-} is formed together with a template effect of the crown to form unique nanowheel Sb_{68}^{8-}. The low tendency of Sb−Sb single-bond formation is the reason for the big differences of the heavier pnictogen Sb toward the lighter group 15 elements in the formation of Zintl-phase modifications.

THEORETICAL ANALYSIS

To further elucidate the bonding and associated properties of Sb_{68}^{8-}, theoretical analysis was conducted. The spin-states, ranging from $S = 0$ to $S = 2$, were verified at the PBE0/def2-tzvp level. The results indicate that the favored state is $S = 0$ (Table S4), for which the structural parameters are in good agreement with the experiments and the maximum deviation of the Sb−Sb bond length is 0.066 Å (Table S2). In addition, the calculated highest occupied molecular orbital−lowest occupied molecular orbital (HOMO−LUMO) gap for Sb_{68}^{8-} is 2.21 eV.

The chemical bonding patterns of Sb_{68}^{8-} (C_i) were conducted by canonical molecular orbital (CMO) analyses and adaptive natural density partitioning (AdNDP) analysis. Our findings revealed the presence of 68 s-type lone pairs and 98 Sb−Sb σ bonds with high occupation numbers (ONs) (see Figure 3a,b). The remaining 16 electrons belong to eight 3c-2e σ bonds with ONs of 1.60/1.70 lel (see Figure 3c), effectively saturating the eight 2-fold-coordinated Sb atoms within the cluster. Consequently, the entire molecular surface is fully covered by σ bonds, ensuring that each Sb atom achieves a triple-coordinated state. The Wiberg bond index of each atom shown in Table S5 also supports the above conclusion.

Electron localization function (ELF) analysis further validated the results of AdNDP analysis. The ELF plot in the plane taken through the surface of the cluster and parallel to the radial plane of Sb_{68}^{8-} clearly indicates the lone pairs of each Sb atom and the localized bonds between the Sb−Sb atoms (Figure 3d). The plots obtained by passing through the center of the cluster, whether parallel or perpendicular to the radial plane of the cluster, confirmed the existence of the Sb lone pairs (Figure S10). Moreover, the CMOs corresponding to the eight 3c-2e σ bonds are shown in Figure S11, which can be divided into two categories: one located inside of the nanotorus and the other ones are outside. Interestingly, in both cases, whether from the results of AdNDP or CMOs, the main contribution to these 3c-2e bonds comes from the p-electrons of the Sb atom in 2-fold-coordination. However, the contribution of the other two atoms cannot be ignored (Table S6), especially for those bonds inside the nanotorus.

The natural bond orbital analysis conducted on the optimized structure of Sb_{68}^{8-} helps us to understand the formation mechanism of this structure. Among these 68 atoms, 4 atoms located inside of the nanotorus carry positive charges (Table S7), and charge transfer occurs between them and the surrounding atoms. Interestingly, starting from the locations of these atoms, the presence of a Sb_7 unit can be detected. Taking into account the aforementioned findings and the typical coordination patterns observed in this structure, one can speculate on the possible assembly mechanism of this structure. The Sb_7 monomers undergo oxidation and then fuse to form an Sb_{17} unit, which in turn further fuses to create an Sb_{34} unit. This Sb_{34} unit then undergoes cyclic assembly under the influence of the [K(18-c-6)]·*tol*·[K(18-c-6)] species as the cationic template, resulting in the formation of nanotorus structure Sb_{68}^{8-}. The Sb_{17} unit contains the classic Sb_{10} unit, which aligns more closely with the Zintl antimony cluster coordination pattern. Moreover, this Sb_{17} unit was also confirmed by mass spectrometric analysis (Figure S6). The analysis above merely offers a glimpse of a potential scenario. In reality, the situation is likely far more intricate and warrants further in-depth investigations.

In summary, the isolation and characterization of a structure-defined, pure antimony-based nanotorus, Sb_{68}^{8-}, introduce a new approach for producing nanotori structures. By using C_{60} as a weak oxidant to fuse the Sb_7^{3-} cages together with the formed K(18-c-6) species, an unprecedented ring structure resembling a carbon nanotorus was observed. According to quantum chemical calculations, the band gap suggests a relatively high level of stability. CMO and AdNDP analyses reveal the presence of s-type lone pairs and 2c-2e σ bonds, while also indicating that the 3c-2e σ bonds effectively saturate the eight two-coordinate Sb atoms, ensuring each antimony atom attains a stable three-coordinated state. These findings are further validated by ELF analysis. The complete molecular surface coverage with σ bonds suggests that Sb_{68}^{8-} could potentially function as nanomaterials akin to semiconductor-like antimony nanotubes. Additionally, CMO analysis indicates that a section of delocalized orbitals is located within the inner region of the nanotorus, containing a cavity with a volume of 14 $Å^3$. This characteristic indicates its potential application in encapsulating chains of metallic atoms or in investigating the optoelectronic properties of metal clusters confined in a manner analogous to molecular sieves. Research on its relevant performance is ongoing.

https://doi.org/10.1021/jacs.4c09102
J. Am. Chem. Soc. 2024, 146, 27977−27982

■ ASSOCIATED CONTENT

Supporting Information

The Supporting Information is available free of charge at https://pubs.acs.org/doi/10.1021/jacs.4c09102.

Detailed experimental procedures, crystallographic supplementation, energy-dispersive X-ray (EDX) spectroscopic analysis, and quantum-chemical studies (PDF)

Accession Codes

CCDC 2351044−2351045 contain the supplementary crystallographic data for this paper. These data can be obtained free of charge via www.ccdc.cam.ac.uk/data_request/cif, or by emailing data_request@ccdc.cam.ac.uk, or by contacting The Cambridge Crystallographic Data Centre, 12 Union Road, Cambridge CB2 1EZ, UK; fax: +44 1223 336033.

■ AUTHOR INFORMATION

Corresponding Author

Zhong-Ming Sun − *State Key Laboratory of Elemento-Organic Chemistry, Tianjin Key Lab for Rare Earth Materials and Applications, School of Materials Science and Engineering, Nankai University, Tianjin 300350, China;* orcid.org/0000-0003-2894-6327; Email: sunlab@nankai.edu.cn

Authors

Yun Zhang − *State Key Laboratory of Elemento-Organic Chemistry, Tianjin Key Lab for Rare Earth Materials and Applications, School of Materials Science and Engineering, Nankai University, Tianjin 300350, China*

Wen-Juan Tian − *Institute of Molecular Science, Shanxi University, Taiyuan 030006, China*

Wei-Xing Chen − *State Key Laboratory of Elemento-Organic Chemistry, Tianjin Key Lab for Rare Earth Materials and Applications, School of Materials Science and Engineering, Nankai University, Tianjin 300350, China*

Manfred Scheer − *Institute of Inorganic Chemistry, University of Regensburg, 93040 Regensburg, Germany;* orcid.org/0000-0003-2182-5020

Complete contact information is available at: https://pubs.acs.org/10.1021/jacs.4c09102

Author Contributions

The manuscript was written through contributions of all authors.

Notes

The authors declare no competing financial interest.

■ ACKNOWLEDGMENTS

This work was supported by the National Natural Science Foundation of China, Grants 22425107 (Z.M.S.), 22371140 (Z.M.S.), 92161102 (Z.M.S.), and 22402108 (W.J.T.).

■ REFERENCES

(1) Münzfeld, L.; et al. Synthesis and properties of cyclic sandwich compounds. *Nature.* **2023**, *620*, 92−96.

(2) Girvin, Z. C.; et al. Foldamer-templated catalysis of macrocycle formation. *Science* **2019**, *366*, 1528−1531.

(3) Li, K.; et al. Dimeric cycloparaphenylenes with a rigid aromatic linker. *Angew. Chem., Int. Ed.* **2021**, *60*, 7649−7653.

(4) Rodríguez-Manzo, J. A.; et al. Magnetism in corrugated carbon nanotori: The importance of symmetry, defects, and negative curvature. *Nano Lett.* **2004**, *4*, 2179−2183.

(5) Kharissova, O. V.; Castañón, M. G.; Kharisov, B. I. Inorganic nanorings and nanotori: State of the art. *J. Mater. Res.* **2019**, *34*, 3998−4010.

(6) Kaiser, K.; et al. An sp-hybridized molecular carbon allotrope, *cyclo*[18]carbon. *Science* **2019**, *365*, 1299−1301.

(7) Sun, L.; et al. On-surface synthesis of aromatic *cyclo*[10]carbon and *cyclo*[14]carbon. *Nature* **2023**, *623*, 972−976.

(8) Gao, Y.; et al. On-surface synthesis of a doubly anti-aromatic carbon allotrope. *Nature* **2023**, *623*, 977−981.

(9) Albrecht, F.; et al. The odd-number *cyclo*[13]carbon and its dimer, *cyclo*[26]carbon. *Science* **2024**, *384*, 677−682.

(10) Liu, J.; et al. Fullerene 'crop circles'. *Nature* **1997**, *385*, 780−781.

(11) Sarapat, P., Hill, J., Baowan, D. A Review of Geometry, Construction and Modelling for Carbon Nanotori. *Appl. Sci.* **2019**, *9*, 2301.

(12) Martel, R.; Shea, H. R.; Avouris, P. Rings of single-walled carbon nanotubes. *Nature* **1999**, *398*, 299.

(13) Sano, M.; et al. Ring closure of carbon nanotubes. *Science* **2001**, *293*, 1299−1301.

(14) Ajori, S.; Sadeghi, F. Design of High-Frequency Carbon Nanotube−Carbon Nanotorus Oscillators for Energy Harvesting: A Molecular Dynamics Study. *Langmuir* **2024**, *40*, 4811−4823.

(15) Zhang, J.; et al. Assembly of ring-shaped phosphorus within carbon nanotube nanoreactors. *Angew. Chem., Int. Ed.* **2017**, *56*, 1850−1854.

(16) Karttunen, A. J.; Linnolahti, M.; Pakkanen, T. A. Icosahedral and Ring-Shaped Allotropes of Phosphorus. *Chem.—Eur. J.* **2007**, *13*, 5232−5237.

(17) Karttunen, A. J.; Linnolahti, M.; Pakkanen, T. A. Icosahedral and Ring-Shaped Allotropes of Arsenic. *ChemPhysChem.* **2007**, *8*, 2373−2378.

(18) Liu, D.; et al. Unusually Stable Helical Coil Allotrope of Phosphorus. *Nano Lett.* **2016**, *16*, 7865−7869.

(19) Cicirello, G.; et al. Two-Dimensional Violet Phosphorus P_{11}: A Large Band Gap Phosphorus Allotrope. *J. Am. Chem. Soc.* **2023**, *145*, 8218−8230.

(20) Hart, M.; et al. One-Dimensional Arsenic Allotropes: Polymerization of Yellow Arsenic Inside Single-Wall Carbon Nanotubes. *Angew. Chem., Int. Ed.* **2018**, *130*, 11823−11827.

(21) Hart, M.; et al. Encapsulation and Polymerization of White Phosphorus Inside Single-Wall Carbon Nanotubes. *Angew. Chem., Int. Ed.* **2017**, *56*, 8144−8148.

(22) Wiegand, T.; et al. Structural Characterization of Phosphorus-Based Networks and Clusters: ^{31}P MAS NMR Spectroscopy and Magnetic Shielding Calculations on Hittorf's Phosphorus. *Chem.—Eur. J.* **2011**, *17*, 8739−8748.

(23) Zhou, X.; et al. Structural and electronic properties of Sb_n (n = 2−10) clusters using density-functional theory. *Phys. Rev. A* **2005**, *72*, 053203.

(24) von Schnering, H. G.; Manriquez, V.; Hönle, W. Bis (tetraphenylphosphonium) Hexadecaphosphide, a Salt Containing the Novel Polycyclic Anion P_{16}^{2-}. *Angew. Chem., Int. Ed.* **1981**, *20*, 594−595.

(25) Baudler, M.; et al. Na_3P_{21} and Li_3P_{21}, the First Polyphosphides with Isolated P Groups. *Angew. Chem., Int. Ed.* **1984**, *23*, 317−318.

(26) Baudler, M.; et al. Li_4P_{26} und Na_4P_{26}, die ersten Salze mit Hexacosaphosphid (4−)-Ionen. *Z. Anorg. Allg. Chem.* **1984**, *518*, 7−13.

(27) Du, S.; et al. Isolation and Characterization of Four Phosphorus Cluster Anions P_7^{3-}, P_{14}^{4-}, $P_{16}^{2-}$and $P_{26}^{4-}$from the Nucleophilic Functionalization of White Phosphorus with 1, 4-Dilithio-1, 3-butadienes. *Chin. J. Chem.* **2019**, *37*, 71−75.

(28) Yue, X. H.; et al. Synthesis, chemical bonding and reactivity of new medium-sized polyarsenides. *Chin. Chem. Lett.* **2024**, *35*, 108907.

(29) Turbervill, R. S. P.; Goicoechea, J. M. From clusters to unorthodox pnictogen sources: solution-phase reactivity of $[E_7]^{3-}$ (E= P−Sb) anions. *Chem. Rev.* **2014**, *114*, 10807−10828.

(30) Hoffmann, S.; Kasinathan, D.; Fässler, T. F. Single Crystals of Rb_4C_{60}: Synthesis and Structure Determination. *Inorg. Chem.* **2010**, *49*, 2577−2579.
(31) Mortensen, K. T.; et al. Strategies for the Diversity-Oriented Synthesis of Macrocycles. *Chem. Rev.* **2019**, *119*, 10288−10317.
(32) Fässler, T. F.; et al. Triple-Decker Triple-Decker Type Coordination of a Fullerene Trianion in $[K([18]\ crown{-}6)]_3$ $[\eta^6,\eta^6{-}C_{60}](\eta^3{-}C_6H_5CH_3)_2$−Single Crystal Structure and Magnetic Properties. *Angew. Chem., Int. Ed.* **2000**, *39*, 2091−2094.
(33) Ganesamoorthy, C.; Wölper, C.; Nizovtsev, A. S.; Schulz, S. Synthesis and Structural Characterization of Magnesium-Substituted-Polystibides $[(LMg)_4Sb_8]$. *Angew. Chem., Int. Ed.* **2016**, *55*, 4204−4209.
(34) Critchlow, S. C.; Corbett, J. D. Homopolyatomic anions of the post transition elements. Synthesis and structure of potassium-crypt salts of the tetraantimonide (2-) and heptaantimonide (3-) anions, $Sb_4^{2-}$and Sb_7^{3-}. *Inorg. Chem.* **1984**, *23*, 770−774.
(35) Pauling, L. Atomic radii and interatomic distances in metals. *J. Am. Chem. Soc.* **1947**, *69*, 542−553.
(36) Cicirello, G.; et al. Two-Dimensional Violet Phosphorus P_{11}: A Large Band Gap Phosphorus Allotrope. *J. Am. Chem. Soc.* **2023**, *145*, 8218−8230.
(37) Xu, Y. H.; et al. Extension and Fusion of Cyclic Polyantimony Units. *J. Am. Chem. Soc.* **2024**, *146*, 15473−15478.

https://doi.org/10.1021/jacs.4c09102
J. Am. Chem. Soc. 2024, 146, 27977−27982